

# Maximum Likelihood Surface Profilometry via Optical Coherence Tomography

Rapp, Joshua; Mansour, Hassan; Boufounos, Petros T.; Orlik, Philip V.; Koike-Akino, Toshiaki; Parsons, Kieran

TR2022-117 October 04, 2022

## Abstract

Optical coherence tomography (OCT) using Fourier domain processing can resolve micrometer-scale depth information. However, the conventional volumetric reconstruction approach is unnecessary for opaque samples with only one reflector per lateral position, and the required sample interpolation degrades performance. In this paper, we show that surface depth profilometry with a Fourier-domain OCT system simplifies to a sinusoidal parameter estimation problem. We derive approximate maximum likelihood estimators for the sample depth and reflectivity, which can easily be computed by backprojecting the data without interpolating. Iterative refinement further improves results at high signal-to-noise ratio (SNR). We demonstrate the performance of the technique compared to the conventional Fourier transform approach on both simulated and experimental data collected with a spectral-domain OCT system. Our results show that maximum likelihood profilometry is fast and more robust to noise than the Fourier approaches at moderate SNR.

*IEEE International Conference on Image Processing (ICIP) 2022*



# MAXIMUM LIKELIHOOD SURFACE PROFILOMETRY VIA OPTICAL COHERENCE TOMOGRAPHY

*J. Rapp, H. Mansour, P. Boufounos, P. Orlik, T. Koike-Akino, K. Parsons*

Mitsubishi Electric Research Laboratories (MERL), Cambridge, MA 02139, USA

## ABSTRACT

Optical coherence tomography (OCT) using Fourier domain processing can resolve micrometer-scale depth information. However, the conventional volumetric reconstruction approach is unnecessary for opaque samples with only one reflector per lateral position, and the required sample interpolation degrades performance. In this paper, we show that surface depth profilometry with a Fourier-domain OCT system simplifies to a sinusoidal parameter estimation problem. We derive approximate maximum likelihood estimators for the sample depth and reflectivity, which can easily be computed by backprojecting the data without interpolating. Iterative refinement further improves results at high signal-to-noise ratio (SNR). We demonstrate the performance of the technique compared to the conventional Fourier transform approach on both simulated and experimental data collected with a spectral-domain OCT system. Our results show that maximum likelihood profilometry is fast and more robust to noise than the Fourier approaches at moderate SNR.

**Index Terms**— Optical coherence tomography, profilometry, maximum likelihood estimation

## 1. INTRODUCTION

Optical coherence tomography (OCT) uses the interference of two beams of light to measure differences in path length. The beat frequency of the interfered light is much lower than the oscillation frequency of light, allowing OCT to achieve fine depth resolution without high-bandwidth electronics. The first demonstrations of OCT were for ocular imaging [1, 2], and the technique has now become standard for that application. Although initially conceived as a method of imaging into an optically transparent volume, OCT has also been used for non-contact *profilometry*, or measuring the topography of an opaque surface, with applications including dermatology [3], varnish monitoring [4], and component inspection in industrial settings [5, 6, 7].

Existing Fourier-domain OCT profilometry approaches are limited in robustness due to the fast Fourier transform (FFT)-based processing used for depth recovery [5, 6]. Because measurements are made with samples uniformly spaced in wavelength, interpolation is required to convert to samples uniformly spaced in wavenumber before the Fourier transform can be applied, and the interpolation introduces errors for high-frequency interference patterns in the presence of noise. Alternative approaches exist for volumetric OCT that avoid interpolation and promote sparsity in the recovered depth [8], but the iterative reconstruction techniques used are much slower than the FFT and do not explicitly impose prior knowledge of the sparsity level when only a single surface is to be recovered.

In this work, we establish a model for depth profile measurements of a single opaque surface using OCT, which we show to

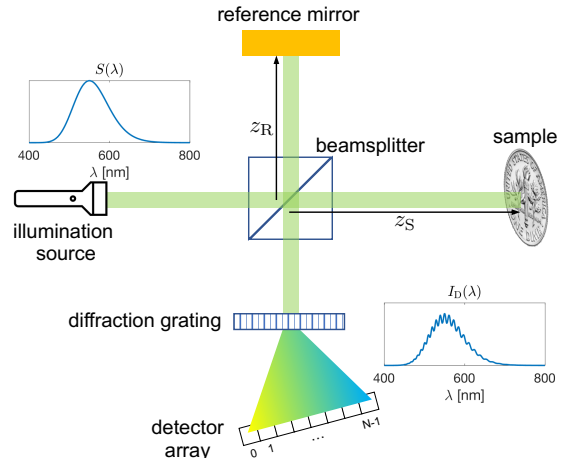


**Fig. 1:** Diagram of an SD-OCT imaging system for profiling an opaque surface. Light from the illumination source with power spectral density  $S(\lambda)$  reflects off the reference mirror and sample, and is recombined by the beamsplitter. The resulting interference signal  $I_D(\lambda)$  is spectrally resolved by the diffraction grating and sampled by the detector array.

be a sinusoidal parameter estimation problem. Our main contribution is the derivation of the maximum likelihood estimator (MLE) of the depth that does not require wavenumber interpolation, thus improving robustness to noise over FFT-based inversion. A discrete approximation to the MLE is found by backprojecting the measurements, and iterative refinement yielding a continuous estimate improves performance and achieves the Cramér–Rao lower bound (CRLB) at high signal-to-noise ratio (SNR). The MLE implementations have runtimes on par with the FFT-based methods. We present the method in the context of a spectral-domain (SD) OCT system, but the same approach would likewise apply to swept-source OCT.

## 2. SINGLE-SURFACE OCT MEASUREMENT MODEL

We first establish the measurement model according to [9] for a single reflector in the sample arm. A sketch of the SD-OCT system is shown in Fig. 1. The light source emits a polychromatic plane wave whose electric field is given as  $E_I = s(k, \omega) \exp[i(kz - \omega t)]$ , with wavenumber  $k = 2\pi/\lambda$ , wavelength  $\lambda$ , temporal frequency  $\omega$ , and amplitude spectrum  $s(k, \omega)$ . The 50/50 beamsplitter splits the incident light into the two arms of the interferometer. After reflecting from the reference mirror, the field entering the beamsplitter from the reference arm is  $E_R = \frac{s(k, \omega)}{\sqrt{2}} r_R \exp[i(2kz_R - \omega t)]$ , which accounts for the  $2z_R$  roundtrip path length in the reference

arm, the reference reflectivity  $r_R$ , and the beamsplitter decreasing the intensity by half. In the sample arm, the electric field is a convolution of the incident light with the depth-dependent sample reflectivity profile. Although in OCT the reflectivity profile is generally continuous or described as a series of discrete reflectors, for a single reflector at depth  $z_S$  with reflectivity  $r_S$ , the electric field is  $E_S = \frac{s(k, \omega)}{\sqrt{2}} r_S \exp[i(2kz_S - \omega t + \phi)]$ , where  $\phi$  accounts for any phase shift incurred by reflection from the sample. The sample and reference fields are recombined by the beamsplitter, and the total intensity at the detector is

$$\begin{aligned} I(k, \omega) &= \frac{1}{2} \langle |E_R + E_S|^2 \rangle \\ &= \frac{1}{4} S(k) \{ r_R^2 + r_S^2 + 2r_R r_S \cos[2k(z_S - z_R) + \phi] \}, \end{aligned} \quad (1)$$

where  $S(k) = \langle |s(k, \omega)|^2 \rangle$  is the illumination source power spectral density (PSD) and the angle brackets  $\langle \cdot \rangle$  denote temporal averaging. Note that (1) has only constant amplitude offset and interference terms—there is no “auto-correlation” term as typically found when multiple surfaces mutually interfere in OCT. In an SD-OCT system, a diffraction grating separates the interference intensity by wavelength. The detector measurement is then the intensity scaled by the detector responsivity  $\rho$ , sampled at wavenumbers  $k_n$  for  $n = 0, \dots, N - 1$ , and corrupted by noise  $v[n]$  that is assumed to be independent and identically distributed (i.i.d.) as a zero-mean Gaussian:

$$I_D[n] = \frac{\rho}{4} S(k_n) \{ r_R^2 + r_S^2 + 2r_R r_S \cos[2k_n(z_S - z_R) + \phi] \} + v[n]. \quad (2)$$

With a few manipulations, the measurement model appears greatly simplified. First, let  $a = r_S/r_R$  be the relative reflectivity and  $d = 2(z_S - z_R)$  be twice the depth of the sample relative to the reference. Then we can rewrite (2) as

$$I_D[n] = \frac{\rho}{4} S(k_n) r_R^2 \{ (1 + a^2) + 2a \cos(k_n d + \phi) \} + v[n]. \quad (3)$$

Inspired by Seck et al. [8], we rearrange to define the data as

$$y[n] \triangleq \frac{2}{\rho r_R^2} \left\{ I_D[n] - \frac{\rho}{4} S(k_n) r_R^2 (1 + a^2) \right\} \quad (4a)$$

$$= S(k_n) a \cos(k_n d + \phi) + w[n], \quad (4b)$$

where  $w[n] = 2v[n]/\rho r_R^2$  is i.i.d. Gaussian noise with mean 0 and variance  $\sigma_w^2$ . The main challenge is estimating the parameter  $d$ , and optionally  $a$  and  $\phi$  from (4b). A second important task is ensuring that the known quantities in (4a) can be calibrated accurately.

### 3. CONVENTIONAL FOURIER APPROACH

Ignoring the PSD factor, we see that (4b) is a pure sinusoid, so applying the Fourier transform should yield a sharp peak in the depth domain. Indeed, finding the position of the peak of the Fourier transform magnitude is effectively the approach taken by other methods using OCT for profilometry. However, OCT systems typically sample the interfered light with uniform wavelength  $\lambda$ , which means the samples are non-uniformly spaced in wavenumber  $k$ . The conventional approach is to interpolate the data and resample uniformly in  $k$ , so that the inverse fast Fourier transform (IFFT) can be used to process the measurements [10, 11].

There are a number of problems with the conventional IFFT approach. First, the interpolation process also propagates the noise to the unsampled wavenumbers, which reduces the robustness to noise, especially for higher frequency interference patterns that correspond to the deepest features of the sample. Second, the IFFT performs unnecessary computation, at the expense of longer computation time, by covering a wider depth range than the limited range that the OCT system can measure, and information for only the positive (or negative frequencies) needs to be recovered. Despite the implication of speed in the FFT, the computation can often be performed more quickly for the limited depth range by explicitly forming the inverse Discrete Fourier Transform (IDFT) matrix.

## 4. MAXIMUM LIKELIHOOD PARAMETER ESTIMATION

Numerous approaches have been established for estimating the parameters of a sinusoid. Here, we modify the procedure for deriving the maximum likelihood estimator (MLE) outlined in [12, Ch. 7.10] to include the PSD  $S(k_n)$  and non-uniform wavenumber sampling, which are ignored in related work [13, 14].

### 4.1. Exact MLE

Given the data vector  $\mathbf{y} = [y[0], \dots, y[N - 1]]^\top$  and assuming white Gaussian noise, the probability density function (PDF) is

$$p(\mathbf{y}; a, d, \phi) = \frac{1}{(2\pi\sigma_w^2)^{N/2}} \exp\left(-\frac{1}{2\sigma_w^2} J_{\mathbf{y}}(a, d, \phi)\right), \quad (5)$$

where

$$J_{\mathbf{y}}(a, d, \phi) = \sum_{n=0}^{N-1} \{y[n] - S(k_n) a \cos(k_n d + \phi)\}^2, \quad (6)$$

and the MLE of  $a, d, \phi$  requires minimizing  $J_{\mathbf{y}}(a, d, \phi)$ . Expanding the cosine in (6) and defining  $\alpha_1 = a \cos(\phi)$  and  $\alpha_2 = -a \sin(\phi)$  yields the quadratic equation

$$\begin{aligned} J'_{\mathbf{y}}(\alpha_1, \alpha_2, d) &= \\ &= \sum_{n=0}^{N-1} \{y[n] - \alpha_1 S(k_n) \cos(k_n d) - \alpha_2 S(k_n) \sin(k_n d)\}^2. \end{aligned} \quad (7)$$

Defining the column vectors  $\mathbf{c} \in \mathbb{R}^N$ ,  $\mathbf{c}_n = S(k_n) \cos(k_n d)$ ,  $\mathbf{s} \in \mathbb{R}^N$ ,  $\mathbf{s}_n = S(k_n) \sin(k_n d)$ ,  $\boldsymbol{\alpha} = [\alpha_1, \alpha_2]^\top$ , and matrix  $\mathbf{H} = [\mathbf{c}, \mathbf{s}]$ , we rewrite (7) as

$$J'_{\mathbf{y}}(\alpha_1, \alpha_2, d) = (\mathbf{y} - \mathbf{H}\boldsymbol{\alpha})^\top (\mathbf{y} - \mathbf{H}\boldsymbol{\alpha}), \quad (8)$$

which is well-known to be minimized by  $\hat{\boldsymbol{\alpha}} = (\mathbf{H}^\top \mathbf{H})^{-1} \mathbf{H}^\top \mathbf{y}$ . Replacing  $\boldsymbol{\alpha}$  with its estimate, we can expand

$$J'_{\mathbf{y}}(\hat{\alpha}_1, \hat{\alpha}_2, d) = \mathbf{y}^\top (\mathbf{I} - \mathbf{H}(\mathbf{H}^\top \mathbf{H})^{-1} \mathbf{H}^\top) \mathbf{y}. \quad (9)$$

To find  $\hat{d}$ , we have to maximize  $\mathbf{y}^\top \mathbf{H}(\mathbf{H}^\top \mathbf{H})^{-1} \mathbf{H}^\top \mathbf{y}$ .

### 4.2. Approximate MLE

To diagonalize  $\mathbf{H}^\top \mathbf{H}$  and simplify inversion, the derivation in [12, Ch. 7.10] relies on a corollary in [15, Appendix A] stating that for  $f_0 \in (0, 1)$ ,

$$\lim_{N \rightarrow \infty} \frac{1}{N} \sum_{n=0}^{N-1} \cos(2\pi f_0 n) = 0. \quad (10)$$

For estimating frequency  $f_0 \in (0, 1)$ , the result approximately holds for large  $N$  so long as  $f_0$  is not too close to 0 or 1. In the OCT parameter estimation problem, we have

$$\begin{aligned} \frac{1}{N} \mathbf{c}^\top \mathbf{s} &= \frac{1}{N} \sum_{n=0}^{N-1} S^2(k_n) \cos(k_n d) \sin(k_n d) \\ &= \frac{1}{2N} \sum_{n=0}^{N-1} S^2(k_n) \sin(2k_n d). \end{aligned} \quad (11)$$

We claim without proof that the approximation  $\frac{1}{N} \mathbf{c}^\top \mathbf{s} \approx 0$  also holds for large enough  $N$  under certain conditions:

1. The  $k_n$  need not be uniformly spaced but should yield values of  $\sin(2k_n d)$  uniformly distributed over  $[-1, 1]$  so that their mean is near zero.
2. The frequency content of  $S^2(k_n)$  should not overlap with  $\sin(2k_n d)$ . This is achieved practically with a slowly-varying PSD and a high-frequency interference signal.

If these conditions are satisfied, we can similarly approximate  $\mathbf{c}^\top \mathbf{c} \approx Q/2$  and  $\mathbf{s}^\top \mathbf{s} \approx Q/2$ , where we define  $Q = \sum_{n=0}^{N-1} S^2(k_n)$ . Thus  $\mathbf{H}^\top \mathbf{H}$  is approximately diagonal, and

$$\begin{aligned} \mathbf{y}^\top \mathbf{H} (\mathbf{H}^\top \mathbf{H})^{-1} \mathbf{H}^\top \mathbf{y} &\approx \frac{2}{Q} ((\mathbf{c}^\top \mathbf{y})^2 + (\mathbf{s}^\top \mathbf{y})^2) \\ &= \frac{2}{Q} \left| \sum_{n=0}^{N-1} y[n] S(k_n) \exp(-ik_n d) \right|^2 \triangleq f(d). \end{aligned} \quad (12)$$

The approximate MLE for  $d$  is thus the value that maximizes (13) as  $\hat{d} = \arg \max_d f(d)$ . Using the same approximations and  $\hat{d}$ , we can then solve  $\hat{\boldsymbol{\alpha}} \approx \frac{2}{Q} [\hat{\mathbf{c}} \hat{\mathbf{s}}]^\top \mathbf{y}$ , from which we get  $\hat{a} \approx \sqrt{\hat{\alpha}_1^2 + \hat{\alpha}_2^2}$  and  $\hat{\phi} \approx \arctan(-\hat{\alpha}_2/\hat{\alpha}_1)$ .

### 4.3. Proposed Solutions: Discrete and Continuous MLEs

The function  $f(d)$  in (13) is multi-modal, so a grid search is needed to find the maximum. We notice that the search can be efficiently performed by matrix-vector multiplication. We define the discrete measurement matrix  $\mathbf{M} \in \mathbb{C}^{N \times M}$ , where  $[\mathbf{M}]_{n,m} = \frac{2}{Q} S(k_n) \exp(ik_n d_m)$  at depths  $d_m$  for  $m = 0, \dots, M-1$ . To avoid missing the true maximum, the depth discretization step size  $\delta_z$  should be smaller than the coherence length, defined in [9] as  $\ell_c = (2 \ln(2)/\pi)(\lambda_0^2/\Delta_\lambda)$  for center wavelength  $\lambda_0$  and full-width at half-maximum (FWHM) wavelength spectral bandwidth  $\Delta_\lambda$ . A discrete approximation to the MLE is found by backprojecting the data and choosing the largest element. Specifically, we compute

$$\mathbf{f} = |\mathbf{M}^* \mathbf{y}|, \quad (14)$$

so that the value of the maximum  $\hat{a} = \max_m \mathbf{f}_m$  is the approximate reflectivity MLE, and the position of the maximum  $\hat{m} = \arg \max_m \mathbf{f}_m$  yields the approximate depth MLE  $\hat{d}^{\text{grid}} = d_{\hat{m}}$ . We note the key difference between applying the Hermitian adjoint of  $\mathbf{M}$  instead of the IDFT is that  $\mathbf{M}$  is explicitly defined for the measured wavenumbers  $k_n$ , avoiding the need for interpolating the measurements that inherently interpolates the noise as well as the signal.

Since the backprojection result  $\hat{d}^{\text{grid}}$  is confined to a discrete grid, the root mean squared error (RMSE) will be limited to  $\sqrt{\delta_z^2}/12$ , assuming uniformly distributed depths [16]. We observe that  $f(d)$  is unimodal near  $\hat{d}^{\text{grid}}$ , so similarly to [17], we iteratively maximize (13) to find a refined continuous estimate  $\hat{d}^{\text{iter}}$ .

We implement  $\hat{d}^{\text{iter}}$  using Brent's minimization method via Matlab's `fminbnd` function, which combines golden section search with parabolic integration [18, Ch. 5]. For the bounding interval, we use  $\hat{d}^{\text{grid}} \pm \ell_c/10$ .

## 5. POWER SPECTRAL DENSITY CALIBRATION

As described in Section 2, although the measurements made by the detector are given as  $I_D[n]$ , the data required for estimation requires the transformation to (4a). Although we have no knowledge of the true values for  $r_R$  or  $\rho$ , we can approximate the data without these scaling factors, which yields relative reflectivity estimates rather than absolute quantities. In a separate calibration measurement, we block the sample arm so the only light reaching the detector is due to the reference arm. Then the intensity at the detector is

$$I_C[n] = \frac{1}{2} \langle |E_R|^2 \rangle = \frac{\rho}{4} S(k_n) r_R^2. \quad (15)$$

If  $r_S \ll r_R$  then  $a^2$  is negligible, so this calibration measurement would be sufficient. However, to compensate for the possibility of samples with higher reflectivity, we normalize the calibration such that  $y[n] \propto I_D[n] - \beta I_C[n]$ , where  $\beta = (\sum_{n=0}^{N-1} I_D[n]) / (\sum_{n=0}^{N-1} I_C[n])$ , which sets the zero-frequency components of the measurement and calibration to be equal.

## 6. NOISE PERFORMANCE

We conducted a simulation of OCT-based profilometry to quantitatively compare the Fourier and MLE approaches. The illumination source was set to have a Gaussian spectrum with center wavelength  $\lambda_0 = 550$  nm and bandwidth  $\Delta_\lambda = 100$  nm, as depicted in Fig. 1. The sample shown in Fig. 2 is a 1-dimensional linear ramp spanning a wide range of depths. The reflectivity at each pixel was set to a constant  $r_S = 0.05$ , and a phase shift was added uniformly at random over  $[0, 2\pi)$ . Measurements were made at 500 wavelengths, and reconstructions were computed for a 25-nm depth resolution and 25- $\mu\text{m}$  maximum depth. We compared the following algorithms:

- **IFFT**: the conventional approach, using linear interpolation of the measurements and inversion via the FFT algorithm;
- **IDFT**: the conventional approach, explicitly specifying the partial inverse DFT matrix for a smaller range of positive depth values;
- **ML-grid**: the depth MLE on a discrete grid;
- **ML-iter**: the depth MLE with iterative refinement.

Table 1 shows the average runtimes of the methods with a multi-core CPU. ML-grid is slightly faster than the IDFT because it avoids the interpolation step, and both methods with explicitly defined matrices are faster than the IFFT. The ML-iter method requires just twice the runtime of the conventional FFT-based approach. In Fig. 3 the depth estimation RMSE is plotted against the SNR averaged over 10 trials. We also plot the square root of the CRLB for  $z = d/2$ ,

**Table 1:** Algorithm runtime comparison (seconds)

IFFT	IDFT	ML-grid	ML-iter
0.0426	0.0173	<b>0.0166</b>	0.0843

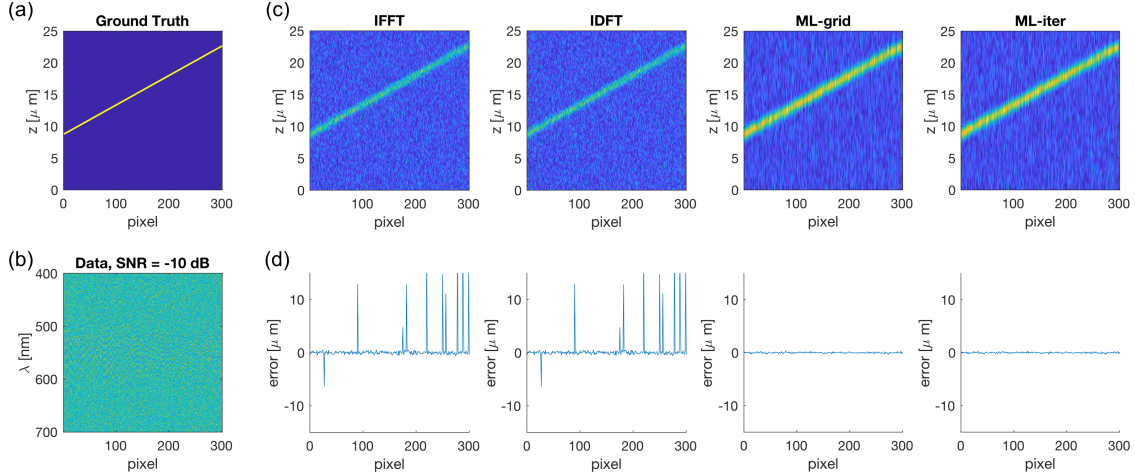


**Fig. 2:** Example depth estimation for (a) a simple linear ramp sample. The measured data (b) is captured at  $-10$  dB SNR. The top row (c) shows the magnitude of the backprojection or inversion for each method. The bottom row (d) shows the estimation error for each method.

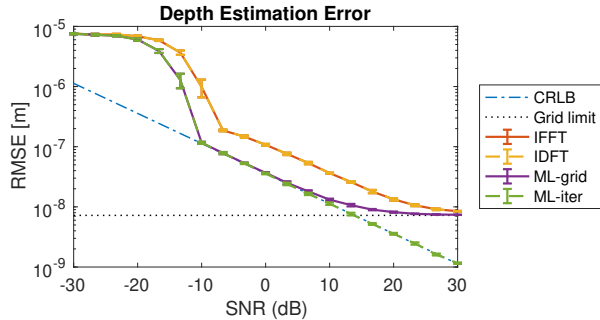


**Fig. 3:** Performance of OCT profilometry algorithms vs SNR. The ML methods outperform Fourier-based methods at all noise levels.

which gives a lower bound on the range accuracy for unbiased estimators. Details of the derivation of the CRLB, which modifies [12, Ch. 3.11] to include  $k_n$  and  $S(k_n)$ , are beyond the scope of this work. Overall, the figures show that the MLE yields better results than the Fourier methods. In fact, the ML methods achieve roughly the same RMSE at 10-dB lower SNR than the Fourier methods. The grid-based and iterative ML methods are essentially the same for 0 dB SNR or lower, whereas the iterative refinement improves estimation performance as the SNR increases and achieves the CRLB above  $-10$  dB SNR. Both the ML-grid and Fourier methods are limited by the discretization of the depth grid size at high SNRs. Based on the noise performance and runtime, ML-grid is the best choice for OCT profilometry for SNR less than 10 dB, while the small runtime penalty for iterative refinement may be a worthwhile tradeoff in high-SNR conditions requiring high precision.

## 7. EXPERIMENTAL VALIDATION

We validate our profilometry approach with the prototype line-field SD-OCT system described in [19]. The illumination source is a green light-emitting diode (Thorlabs M530L4) with 530-nm center wavelength and 35-nm FWHM bandwidth, which yields a theoretical axial resolution of approximately  $3.5 \mu\text{m}$  [10]. The sample is

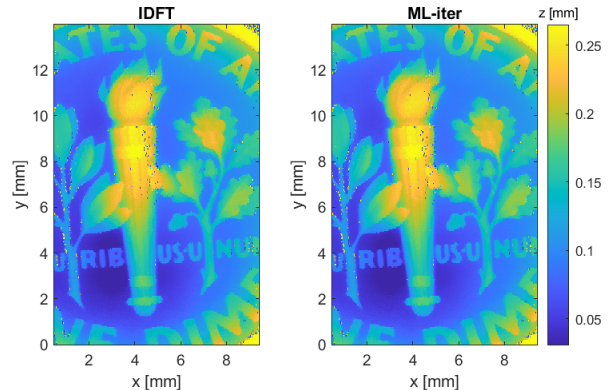


**Fig. 4:** Experimental results for OCT profilometry of a US dime.

a US dime (ten-cent coin). Based on the results of the simulation, we present only reconstructions using the ML-iter and IDFT methods in Fig. 4. It is difficult to visually distinguish the performance, with both the ML and Fourier methods producing good estimates across most of the sample. Errors are clustered around regions of low local SNRs, such as the sides, where the illumination intensity falls off, and at object edges, from which the specular surface reflects little light toward the sensor. In future work, advanced image processing algorithms or experimental modifications will improve the surface profile estimate, and OCT-based estimates can be compared to contact-based ground-truth measurements.

## 8. CONCLUSION

Non-contact profilometry using an OCT system does not require full volume reconstruction. In this paper, we demonstrated that maximum likelihood reconstruction of a single surface could be computed efficiently and was more robust to noise than FFT-based processing of interpolated measurements. The speed and robustness of the MLE are promising for a wide variety of industrial applications. Future work will improve experimental data collection and address MLE approaches for samples with more than one reflecting surface.

## 9. REFERENCES

- [1] D. Huang, E. A. Swanson, C. P. Lin, J. S. Schuman, W. G. Stinson, W. Chang, M. R. Hee, T. Flotte, K. Gregory, C. A. Puliafito, and J. G. Fujimoto, "Optical coherence tomography," *Science*, vol. 254, no. 5035, pp. 1178–1181, 1991.
- [2] A. Fercher, C. Hitzenberger, G. Kamp, and S. El-Zaiat, "Measurement of intraocular distances by backscattering spectral interferometry," *Optics Communications*, vol. 117, no. 1-2, pp. 43–48, May 1995.
- [3] G. Haeusler and M. W. Lindner, "'Coherence radar' and 'Spectral radar' - new tools for dermatological diagnosis," *Journal of Biomedical Optics*, vol. 3, no. 1, pp. 21–31, Jan. 1998.
- [4] S. Lawman and H. Liang, "High precision dynamic multi-interface profilometry with optical coherence tomography," *Applied Optics*, vol. 50, no. 32, pp. 6039–6048, Nov. 2011.
- [5] T. Endo, Y. Yasuno, S. Makita, M. Itoh, and T. Yatagai, "Profilometry with line-field Fourier-domain interferometry," *Optics Express*, vol. 13, no. 3, pp. 695–701, Feb. 2005.
- [6] N. J. Suliali, P. Baricholo, P. H. Neethling, and E. G. Rohwer, "Development of a low-cost, 11  $\mu\text{m}$  spectral domain optical coherence tomography surface profilometry prototype," in *Optical Measurement Systems for Industrial Inspection X*. June 2017, vol. 10329, pp. 666–673, SPIE.
- [7] O. Atalar, D. S. Millar, P. Wang, T. Koike-Akino, K. Kojima, P. V. Orlik, and K. Parsons, "Spectrally sparse optical coherence tomography," *Optics Express*, vol. 28, no. 25, pp. 37798, Dec. 2020.
- [8] H. L. Seck, Y. Zhang, and Y. C. Soh, "Optical coherence tomography by using frequency measurements in wavelength domain," *Optics Express*, vol. 19, no. 2, pp. 1324–1334, Jan. 2011.
- [9] J. A. Izatt and M. A. Choma, "Theory of optical coherence tomography," in *Optical Coherence Tomography: Technology and Applications*, W. Drexler and J. G. Fujimoto, Eds., Biological and Medical Physics, Biomedical Engineering, pp. 47–72. Springer, Berlin, Heidelberg, 2008.
- [10] M. Wojtkowski, V. J. Srinivasan, T. H. Ko, J. G. Fujimoto, A. Kowalczyk, and J. S. Duker, "Ultrahigh-resolution, high-speed, Fourier domain optical coherence tomography and methods for dispersion compensation," *Optics Express*, vol. 12, no. 11, pp. 2404–2422, May 2004.
- [11] K. Zhang and J. U. Kang, "Graphics processing unit accelerated non-uniform fast Fourier transform for ultrahigh-speed, real-time Fourier-domain OCT," *Optics Express*, vol. 18, no. 22, pp. 23472–23487, Oct. 2010.
- [12] S. M. Kay, *Fundamentals of Statistical Signal Processing: Estimation Theory*, Prentice-Hall, Inc., Upper Saddle River, NJ, USA, 1993.
- [13] C. Ma and A. Wang, "Signal processing of white-light interferometric low-finesse fiber-optic Fabry–Perot sensors," *Applied Optics*, vol. 52, no. 2, pp. 127–138, Jan. 2013.
- [14] C. Li, S. Chen, and Y. Zhu, "Maximum likelihood estimation of optical path length in spectral interferometry," *Journal of Lightwave Technology*, vol. 35, no. 22, pp. 4880–4887, Nov. 2017.
- [15] P. Stoica, R. Moses, B. Friedlander, and T. Söderström, "Maximum likelihood estimation of the parameters of multiple sinusoids from noisy measurements," *IEEE Transactions on Acoustics, Speech, and Signal Processing*, vol. 37, no. 3, pp. 378–392, Mar. 1989.
- [16] R. M. Gray and D. L. Neuhoff, "Quantization," *IEEE Transactions On Information Theory*, vol. 44, no. 6, 1998.
- [17] D. Rife and R. Boorstyn, "Single tone parameter estimation from discrete-time observations," *IEEE Transactions on Information Theory*, vol. 20, no. 5, pp. 591–598, Sept. 1974.
- [18] R. P. Brent, *Algorithms for Minimization Without Derivatives*, Prentice-Hall, Inc., Englewood Cliffs, NJ, USA, 1973.
- [19] C. Yurdakul, D. S. Millar, H. Mansour, P. Wang, K. Kojima, T. Koike-Akino, K. Parsons, and P. V. Orlik, "Line-field coherent sensing with LED illumination," arXiv:2202.12161v1, Feb. 2022.